Exciton-Polariton Fano Resonance Driven by Second Harmonic Generation

Yafeng Wang,[1] Liming Liao,[1] Tao Hu,[1] Song Luo,[1] Lin Wu,[1] Jun Wang,[1] Zhe Zhang,[1] Wei Xie,[1] Liaoxin Sun,[1] A. V. Kavokin,[2,3,4] Xuechu Shen,[1] and Zhanghai Chen[1,*]

[1]*State Key Laboratory of Surface Physics, Key Laboratory of Micro and Nano Photonic Structures (Ministry of Education), Department of Physics, Collaborative Innovation Center of Advanced Microstructures, Fudan University, Shanghai 200433, China, and Collaborative Innovation Center of Advanced Microstructures, Nanjing University, Nanjing Jiangsu 210093, China*

[2]*University of Southampton, Highfield, Southampton SO249QH, United Kingdom*

[3]*SPIN-CNR, Viale del Politechnico 1, I-00133 Rome, Italy*

[4]*Spin Optics Laboratory, St-Petersburg State University, 1 Ulianovskaya, St-Petersburg, 198504, Russia*

(Received 12 October 2016; published 8 February 2017)

Angle-resolved second harmonic generation (SHG) spectra of ZnO microwires show characteristic Fano resonances in the spectral vicinity of exciton-polariton modes. We observe a resonant peak followed by a strong dip in SHG originating from the constructive and destructive interference of the nonresonant SHG and the resonant contribution of the polariton mode. It is demonstrated that the Fano line shape, and thus the Fano asymmetry parameter q, can be tuned by the phase shift of the two channels. We develop a model to calculate the phase-dependent q as a function of the radial angle in the microwire and achieve a good agreement with the experimental results. The deduced phase-to-q relation unveils the crucial information about the dynamics of the system and offers a tool for control on the line shape of the SHG spectra in the vicinity of exciton-polariton modes.

DOI: 10.1103/PhysRevLett.118.063602

Fano resonances are fingerprints of quantum interference as pointed out in the pioneering work by Fano [1]. A Fano resonance originates from the interference between a discrete state and a continuum of quantum states, giving rise to a characteristic asymmetric emission line shape. First introduced to describe atomic photoionization [1,2], the exploration of this important phenomenon and the underlying physics have been extended to the field of photonic crystals [3–5], plasmonic devices [6,7], metamaterials [8–10], fiber-cavity systems [11], Raman scattering [12], the nonlinear optical regime [13–15], etc., [16–21]. The Fano line shape is considered as a unique asymmetric spectral response, and its tunability in a discrete-continuum-coupled quantum system provides great opportunities for developing optronic devices such as on-chip optical sensors and switching devices [10,16,21]. A crucial parameter that characterizes a Fano resonance is the spectroscopic asymmetry factor q. The spectral reflectance and transmittance at resonance of a discrete-continuum-coupled quantum system depend strongly on this asymmetry parameter q. Recently, a universal approach for manipulating the asymmetry parameter q of a Fano line shape, i.e., phase shift tuning of the discrete state, has been introduced by Ott *et al.* in an atomic system [18,19]. It is expected that, in an optical resonator with discrete optical modes, this approach of phase shift tuning can be easily achieved by varying the shape, size, etc., of resonators.

In microcavities with semiconductor gain media, well-defined cavity exciton-polariton modes dominate the optical properties near the band-edge energy. As half-light–half-matter quasiparticles, exciton polaritons are formed due to the strong coupling of photons and excitons. These quasiparticles have a bosonic nature and a tunable effective mass. From the point of view of cavity quantum electrodynamics, polariton modes in a semiconductor microcavity not only provide a playground for simulating cold atom physics, such as Bose-Einstein condensation, super fluidity, etc., in the solid state environment at elevated temperatures [22–26], but also can serve as discrete states for Fano resonance studies. However, despite its great importance for optoelectronics, the Fano resonance in a cavity polariton system is yet to be demonstrated. The main challenge is finding coherent broad continuum states that can efficiently couple with a cavity polariton state. Nonlinear optical effects, such as second harmonic generation (SHG) in a bulk semiconductor crystal, may provide a channel for the preparation of coherent continuum states. Efforts have been made to study the polariton-SHG interaction in GaAs-based microcavities, and two-photon absorption of polaritons using SHG excitation has been observed [27]. However, no sign of Fano resonance has been reported so far.

Here we report on the observation of polariton Fano resonances in SHG spectra of ZnO microwires. As a wide band-gap semiconductor, ZnO has not only a large exciton binding energy [~60 meV at room temperature (RT)] but also large nonlinear coefficients, providing both stable cavity exciton-polariton states and a strong SHG continuum at RT. In the past few years, these two aspects have attracted much attention. Striking features of cavity polariton effects, such as ultrastrong exciton-photon coupling [25], polariton lasing at RT and above RT [26,28–30],

polariton parametric scattering [28], polariton-polariton coupling [31], polariton-phonon interaction [32,33], and evaporative cooling of polaritons [34], etc., have been revealed. On the other hand, the SHG effect of ZnO has also been well explored, including exciton-enhanced SHG [35], SHG that is influenced by crystalline structure, dimensions, grains, and doping [36], second harmonic polaritons [37], etc., Taking advantage of coherent polariton states and SHG continuum states with comparable strength in ZnO, Fano resonances with high coupling coefficiency can be expected. In whispering gallery mode resonators of ZnO, the gain medium acts also as the optical cavity, which provides a unique system for the large overlap in real space of a discrete cavity polariton mode and broad SHG continuum. We reveal the Fano resonances between polariton modes and SHG. The angle-resolved spectroscopy enables us to observe the clear Fano fingerprint. Symmetric and asymmetric line shapes are obtained due to the controllable phase shift of the polariton mode with respect to the continuum states. The phase-dependent q has been extracted from these data.

Figure 1(a) shows the scanning electron microscope (SEM) of a typical ZnO microwire. The diameter of the ZnO microwire is about 1.6 μm, and the c axis is parallel to the longitudinal crystal axis. Figure 1(b) shows a schematic configuration of our experiment. A ZnO microwire was laid on a glass substrate, the fundamental laser beam was focused on the back, and SHG was detected from the front side. Angle-resolved spectra measurements were performed along the angles θ and ϕ by using a Princeton Instrument SP 750 spectrometer with the wavelength resolution of 0.02 nm and a charge-coupled detector of Pixis 100. The detection scheme is shown in Scheme S1 in Supplemental Material [38]. For the SHG measurements, femtosecond laser pulses from a Ti:sapphire laser (150 fs) served as the fundamental light source. The repetition rate is 80 MHz, and the wavelength can be tuned from 700 to 1000 nm. All the experiments were performed at RT.

Figure 1(c) shows the energy dispersion of 29th and 28th TM-polarized (electric field is parallel to the c axis) polariton modes under continuous He-Cd laser (325 nm) excitation. The polariton modes observed in the PL spectra can be fitted with Lorentzian functions (shown in Fig. S1) [38]. The 29th polariton mode has a quality factor of ~2430, which is obtained from the ratio $E/\Delta E$, where $\Delta E = 1.3$ meV is the full width at half maximum (FWHM). The pure SHG radiation without coupling with a polariton mode is displayed in Figs. S2(a) and S2(b) in Ref. [38]. SHG spectra measured with the polarization resolution are shown in Fig. S2(c). The line shape of SHG also can be well fitted by using a Lorentzian function, giving the FWHM $\approx$ 12 meV. It should be emphasized that the FWHM of SHG is about 9.2 times larger than that of the polariton; therefore, it makes the background SHG play the role of continuum states and the polariton mode be a discrete state.

In our experiment, the power of the fundamental wave is set to be 3.4 mJ/cm^2 in order to minimize the PL emission that may interfere with the SHG radiation. The wavelength of SHG is set to resonate with a polariton mode. The resulting θ-resolved spectra are shown in Fig. 2(a). Both TE and TM polariton modes were taken into account first, as the energies of the 28th TE and 29th TM modes at $\theta = 0°$ are quite close: 3.157 and 3.169 eV, respectively (see Fig. S5 in Ref. [38]), while only the TM polariton mode was found to be populated due to the polarization selection

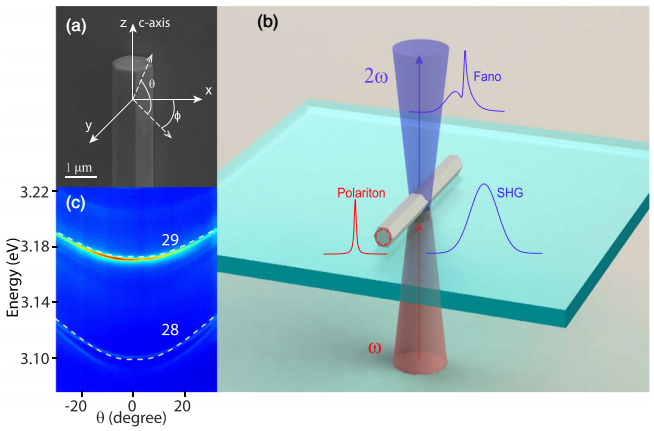

FIG. 1. (a) The SEM of a typical ZnO microwire. The angles defined as θ and ϕ represent the two detection planes of the angle-resolved spectra. (b) The fundamental light wave irradiates the ZnO microwire from the back of the glass, and the SHG radiation is emitted from the top of the wire. (c) The dispersion of the 28th and 29th TM-polarized polariton modes, fitting with the white dashed lines.

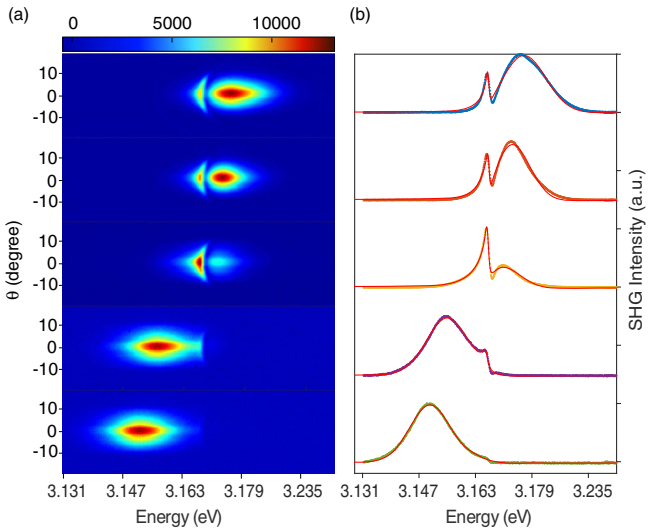

FIG. 2. (a) Angle θ-resolved SHG spectra with the peak at 3.175, 3.172, 3.169, 3.155, and 3.151 eV from top to bottom. (b) The corresponding line curves at $\theta = 0°$, fitting with the red solid lines by Eq. (1).

rules. When the broad SHG band scans from the lower energy side near 3.169 eV, there appears a strong peak accompanied by a dip adjacent to it. This is a signature of Fano resonance. The corresponding spectra at $\theta = 0°$ are shown in Fig. 2(b). Their asymmetric line shapes signify that SHG and the polariton mode are not independent in ZnO. Instead, they interfere with each other to form a new hybrid emission in the vicinity of the resonance. In this regime, the polariton and SHG not only are highly coherent but also have a large overlap in real space which results in a large coupling efficiency.

Here we need to mention that, in the absence of the polariton mode, SHG has a broad symmetric line shape with its intensity independent of angle ϕ (shown in Fig. S3 in Ref. [38]). However, once the SHG and polariton are in the regime of Fano resonance, the asymmetric line shape varies with the angle ϕ, as shown by the angle ϕ-resolved spectra of SHG resonated with the 29th polariton mode in Fig. 3(a) (the SHG-polariton mode resonance spectra for the 28th and 27th modes are shown in Fig. S4 in Ref. [38]). The pattern shows that the spectra intensity distribution depends on the detection angle ϕ. As the ϕ changes from −30° to 30°, the positions of the dip (dark) and the peak (bright) swap. This phenomenon indicates that interference between the SHG and polariton mode controls the line shape of the spectra. To show distinctly the line shape variation with varying the angle ϕ, we plot the spectral profiles at some typical angles (−27°, −15°, −8.3°, 0°, 7.7°, 15°, and 27°) in Fig. 3(c) (black dotted curves). This phenomenal line shape under Fano resonance condition is given by

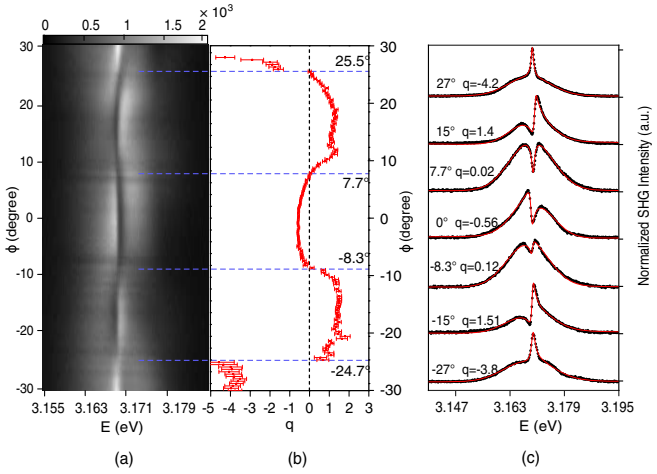

FIG. 3. (a) Angle ϕ-resolved spectral patterns. The SHG and polariton mode are resonant at 3.169 eV. (b) q values at each angle are obtained by fitting each line profile. The dashed lines are the boundaries where q changes sign. (c) The typical line profiles taken at $\phi = -27°$, −15°, −8.3°, 0°, 7.7°, 15°, and 27° from pattern (a). The black dotted lines are experimental data, and the red solid lines are fitted data. These curves show the different line shapes resulting from the Fano coupling in the system.

$$I = A_F\left(\frac{(\epsilon + q)^2}{\epsilon^2 + 1} - 1\right) + I_b, \quad (1)$$

where I is the output emission spectral intensity. $A_F[(\epsilon + q)^2/(\epsilon^2 + 1) - 1]$ is the Fano resonance term [1]. A_F is the amplitude coefficient. $\varepsilon = 2(\omega - \omega_r)/\Gamma_p$ is the reduced energy, where ω_r is the resonant frequency and Γ_p is the linewidth of the polariton mode. q denotes the Fano asymmetry factor. The second term I_b is the Lorentzian background contributed by the broad continuum states populated by SHG. The line profiles are fitted well using Eq. (1) (red solid curves), and the q values are obtained for each curve. According to Fano, the dimensionless parameter q introduced in Eq. (1) manifests the ratio of the transition probabilities to the polariton state and to the continuous SHG states, which can be either positive or negative depending on the phase difference of the two transition channels. It is this parameter q that governs the resonant line shape. In Fig. 3(c), the spectra at −15°, 0°, and 15° show characteristic asymmetric line shapes; in these cases, the probabilities for these two transition channels are similar, leading to q near ±1. The spectra at angles −8.3° and 7.7° show a nearly symmetric line shape with a dip at the center, which is known as antiresonance or the EIT-like effect in other systems [8]. This is because the value of q approaches zero here, in which case the optical transition to the continuum SHG states dominates. When it comes to −27° and 27°, the line shapes show a peak at the resonant position, due to the large absolute q values of -3.8 ± 0.3 and -4.2 ± 0.4. This q variation is a direct consequence of the phase-difference changes in the interference between the two channels; the above results indicate that the relative phase difference, and hence the degree of asymmetry of the resonant line shape, depends on the angle ϕ. In order to extract the phase-difference dependence of the polariton-SHG Fano resonance, we plot the q values for each ϕ in Fig. 3(b). It is noticeable that q is positive from −24.7° to −8.3° (and 7.7° to 25.5°) and negative in other areas. Remarkably, q shows a symmetric dependence on the angle ϕ. As far as we know, the SHG background generated through such a ZnO microwire can be considered as light radiating from a hexagonal medium, which has a phase that hardly changes with angle ϕ. Therefore, we attribute the variation of q with angle ϕ to the phase shift of the polariton channel.

To describe the phase of the polariton mode quantitatively, we calculate the near field electric field distribution for the TM-polarized 29th polariton mode in Fig. 4(a) using the finite element analysis method [38]. The x and y are real space coordinates. In our simulation, the polariton effect manifests itself in the wavelength dependence of the effective refractive index [25]. One can see in Fig. 4(a) that the electric field (including its phase) of the polariton mode has a strong dependence on the angle ϕ. The inset in Fig. 4(a) shows the equiphase surface (the black curves) for

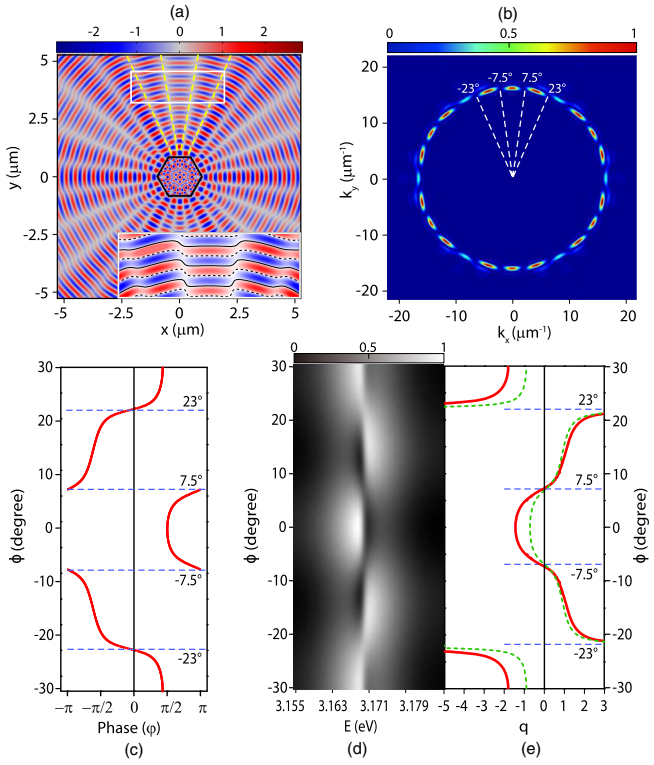

FIG. 4. (a) The electric field distribution pattern for the 29th polariton mode in real space calculated using the finite element analysis. Inset: The equiphase surface is marked by the dashed and solid lines for the white rectangle area. (b) The Fourier transform of pattern (a). The dashed lines mark the angles where the phase of the emission electric field in pattern (a) changes sign. (c) The phase φ vs ϕ curve obtained with the use of the phase information in (a). (d) The theoretical pattern calculated by using Eq. (3) with A_p/Γ_p being the amplitude against ϕ obtained from (b) and A_s/Γ_s being the same order of A_p/Γ_p. Γ_p and Γ_s are the FWHM (in the frequency domain) of the 29th polariton mode (1.3 meV) and SHG (12 meV), respectively. (e) The q variation obtained by fitting each line of pattern (d) (red solid line) and $q(\varphi) = -\cot(\varphi/2)$ (green dashed line).

the area in the white rectangle. The phase is zero for the dashed lines and π for the solid lines. In order to know precisely the angle corresponding to the boundary separating opposite phases in the momentum space, we applied the Fourier transform for Fig. 4(a) and obtained the far field emission pattern in Fig. 4(b). The horizontal and vertical coordinates are wave vectors projections of k_x and k_y, respectively. The emission pattern shows a circle consisting of many bright maxima characterized by the identical $|k|\left(\sqrt{k_x^2 + k_y^2}\right)$. The gaps between the adjacent bright spots indicate the boundaries where the phase changes sign. Using Figs. 4(a) and 4(b), we have obtained the dependence of the phase φ on the angle ϕ shown in Fig. 4(c). The marked angles, consistent with those in Fig. 4(b), indicate that the phase stays above $\pi/2$ from $-7.5°$ to $7.5°$, then it changes almost $-\pi$ and stays nearly below $-\pi/2$ from $7.5°$ to $23°$ (and $-7.5°$ to $-23°$), and finally it goes sharply to $\pi/2$ beyond $23°$ or $-23°$.

To obtain more insight on the coupling features mentioned above, here we model the experiment in more detail. The time-dependent electric field can be expressed as

$$E(t) = A_p e^{-(\Gamma_p/2)t} e^{-i\omega_p t + i\varphi} + A_s e^{-(\Gamma_s/2)t} e^{-i\omega_s t}, \quad (2)$$

where A_p and A_s are the emission field amplitude of the polariton state and SHG states, respectively. Γ_p and Γ_s are the decay rates of the two channels, respectively. ω_p and ω_s are frequencies of the two channels. φ is the phase shift of the polariton state. In the frequency domain, the frequency-dependent electric field intensity I_ω is obtained via the Fourier transformation of Eq. (2), which yields

$$I_\omega = |E(\omega)|^2 \propto \left(\frac{A_p^2}{\Gamma_p^2(1+\varepsilon_p^2)} + \frac{A_s^2}{\Gamma_s^2(1+\varepsilon_s^2)} + 2\frac{A_p A_s}{\Gamma_p \Gamma_s} \frac{(1+\varepsilon_p\varepsilon_s)\cos\varphi + (\varepsilon_p - \varepsilon_s)\sin\varphi}{(1+\varepsilon_p^2)(1+\varepsilon_s^2)} \right). \quad (3)$$

Here $\varepsilon_p = (\omega - \omega_p)/\Gamma_p$ and $\varepsilon_s = (\omega - \omega_s)/\Gamma_s$. The first and the second terms in large parentheses describe the symmetric Lorentzian shape in the frequency domain originating from the polariton mode and SHG, respectively, and the last term describes the coupling strength between these two characters. Using this equation, we simulated the emission pattern as shown in Fig. 4(d), and the effective q is obtained by fitting every line profile in Fig. 4(e) (red solid curve) using Eq. (1). These theoretical results show good agreement with the experimental results shown in Fig. 3(b). Thereafter, for the sake of simplicity, Γ_s is approximated to infinity, which means SHG is replaced by an infinitely broad background state, and the amplitude of the background state is much larger than that of the discrete state ($A_s/\Gamma_s \gg A_p/\Gamma_p$), which provides a strong enough continuum of states. Thus, the correspondence between q and the phase shift φ is obtained as (more details are in [38])

$$q = -\cot\frac{\varphi}{2}. \quad (4)$$

This result means that by manipulating the phase φ of the discrete state one can directly alter the asymmetry parameter q, which is similar to the results obtained in an atomic system [18]. Knowing this, and with the use of the dependence of the phase φ on the angle ϕ in Fig. 4(c), we mapped the angle ϕ into the q parameter and plotted the curve of q vs ϕ in Fig. 4(e) (green dashed curve). It agrees with the experimental values of q well. This indicates that Eq. (4) is sufficiently accurate in our problem. Having an analytical expression, we are able to understand the variation of the complex SHG line shape with the angle ϕ. The phase ϕ-sensitive Fano resonance exhibits rich physics for the polariton-SHG coupling.

In conclusion, we have experimentally demonstrated and theoretically analyzed a Fano resonance in the SHG radiation spectra of an individual semiconductor microwire. In the coupling between the exciton polariton and SHG, the polariton mode serves as a discrete state and SHG serves as the continuum. Angle-resolved spectra exhibit pronounced variation of the Fano line shape, resulting from the phase shift of the cavity polariton mode. These observations are important for the precision control of the Fano line shapes in semiconductor microwire.

The work is funded by National Science Foundation for China (No. 11225419, No. 91321311, No. 11674069, and No. 11474297) and Program of Shanghai Subject Chief Scientist (No. 14XD1400200). A. V. K. thanks the HORIZON 2020 RISE project CoExAn (Grant No. 644076) and the Russian Foundation for Basic Research, Grant No. 15-59-30406-PT.

Y. W. and L. L. contributed equally to this work.

*zhanghai@fudan.edu.cn

[1] U. Fano, Phys. Rev. **124**, 1866 (1961).
[2] A. E. Miroshnichenko, S. Flach, and Y. S. Kivshar, Rev. Mod. Phys. **82**, 2257 (2010).
[3] I. V. Soboleva, V. V. Moskalenko, and A. A. Fedyanin, Phys. Rev. Lett. **108**, 123901 (2012).
[4] P. T. Valentim, J. P. Vasco, I. J. Luxmoore, D. Szymanski, H. Vinck-Posada, A. M. Fox, D. M. Whittaker, M. S. Skolnick, and P. S. S. Guimarães, Appl. Phys. Lett. **102**, 111112 (2013).
[5] M. V. Rybin, A. B. Khanikaev, M. Inoue, K. B. Samusev, M. J. Steel, G. Yushin, and M. F. Limonov, Phys. Rev. Lett. **103**, 023901 (2009).
[6] A. Christ, Y. Ekinci, H. H. Solak, N. A. Gippius, S. G. Tikhodeev, and O. J. F. Martin, Phys. Rev. B **76**, 201405 (2007).
[7] Y. Vardi, E. Cohen-Hoshen, G. Shalem, and I. Bar-Joseph, Nano Lett. **16**, 748 (2016).
[8] S. Zhang, D. A. Genov, Y. WangM. Liu, and X. Zhang, Phys. Rev. Lett. **101**, 047401 (2008).
[9] B. Luk'yanchuk, N. I. Zheludev, S. A. Maier, N. J. Halas, P. Nordlander, H. Giessen, and C. Chong, Nat. Mater. **9**, 707 (2010).
[10] C. Wu, A. B. Khanikaev, R. Adato, N. Arju, A. A. Yanik, H. Altug, and G. Shvets, Nat. Mater. **11**, 69 (2011).
[11] J. Göres, D. Goldhaber-Gordon, S. Heemeyer, M. A. Kastner, H. Shtrikman, D. Mahalu, and U. Meirav, Phys. Rev. B **62**, 2188 (2000).
[12] S. Piscanec, M. Cantoro, A. C. Ferrari, J. A. Zapien, Y. Lifshitz, S. T. Lee, S. Hofmann, and J. Robertson, Phys. Rev. B **68**, 241312 (2003).
[13] M. Kroner *et al.*, Nature (London) **451**, 311 (2008).
[14] H. Mashiko, T. Yamaguchi, K. Oguri, A. Suda, and H. Gotoh, Nat. Commun. **5**, 5599 (2014).
[15] W. Zhang, A. O. Govorov, and G. W. Bryant, Phys. Rev. Lett. **97**, 146804 (2006).
[16] L. Stern, M. Grajower, and U. Levy, Nat. Commun. **5**, 4865 (2014).
[17] A. Zielinski, V. P. Majety, S. Nagele, R. Pazourek, J. Burgdorfer, and A. Scrinzi, Phys. Rev. Lett. **115**, 243001 (2015).
[18] C. Ott, A. Kaldun, P. Raith, K. Meyer, M. Laux, J. Evers, C. H. Keitel, C. H. Greene, and T. Pfeifer, Science **340**, 716 (2013).
[19] A. Kaldun, C. Ott, A. Blattermann, M. Laux, K. Meyer, T. Ding, A. Fischer, and T. Pfeifer, Phys. Rev. Lett. **112**, 103001 (2014).
[20] T. T. Tang *et al.*, Nat. Nanotechnol. **5**, 32 (2010).
[21] K. Nozaki, A. Shinya, S. Matsuo, T. Sato, E. Kuramochi, and M. Notomi, Opt. Express **21**, 11877 (2013).
[22] C. Weisbuch, M. Nishioka, A. Ishikawa, and Y. Arakawa, Phys. Rev. Lett. **69**, 3314 (1992).
[23] M. Zamfirescu, A. Kavokin, B. Gil, G. Malpuech, and M. Kaliteevski, Phys. Rev. B **65**, 161205 (2002).
[24] A. V. Kavokin and G. Malpuech, *Cavity Polaritons* (Elsevier, Amsterdam, 2003), Vol. 32.
[25] L. Sun, Z. Chen, Q. Ren, K. Yu, L. Bai, W. Zhou, H. Xiong, Z. Q. Zhu, and X. Shen, Phys. Rev. Lett. **100**, 156403 (2008).
[26] F. Li *et al.*, Phys. Rev. Lett. **110**, 196406 (2013).
[27] J. Schmutzler, M. Aßmann, T. Czerniuk, M. Kamp, C. Schneider, S. Höfling, and M. Bayer, Phys. Rev. B **90**, 075103 (2014).
[28] W. Xie, H. Dong, S. Zhang, L. Sun, W. Zhou, Y. Ling, J. Lu, X. Shen, and Z. Chen, Phys. Rev. Lett. **108**, 166401 (2012).
[29] D. Xu, W. Xie, W. Liu, J. Wang, L. Zhang, Y. Wang, S. Zhang, L. Sun, X. Shen, and Z. Chen, Appl. Phys. Lett. **104**, 082101 (2014).
[30] Q. Duan *et al.*, Appl. Phys. Lett. **103**, 022103 (2013).
[31] Y. Wang *et al.*, Phys. Rev. B **91**, 121301(R) (2015).
[32] W. Liu *et al.*, Phys. Rev. B **89**, 201201(R) (2014).
[33] A. Trichet, L. Sun, G. Pavlovic, N. A. Gippius, G. Malpuech, W. Xie, Z. Chen, M. Richard, and Le Si Dang, Phys. Rev. B **83**, 041302(R) (2011).
[34] J. Wang *et al.*, Phys. Rev. B **91**, 165423 (2015).
[35] M. Lafrentz, D. Brunne, A. V. Rodina, V. V. Pavlov, R. V. Pisarev, D. R. Yakovlev, A. Bakin, and M. Bayer, Phys. Rev. B **88**, 235207 (2013).
[36] M. C. Larciprete and M. Centini, Appl. Phys. Rev. **2**, 031302 (2015).
[37] M. G. Capeluto, G. Grinblat, M. Tirado, D. Comedi, and A. V. Bragas, Opt. Express **22**, 5341 (2014).
[38] See Supplemental Material at http://link.aps.org/supplemental/10.1103/PhysRevLett.118.063602 for more details of the detection configuration, exciton-polariton dispersion spectra, the SHG information and the theoretical calculation, which includes Refs. [39–42].
[39] J. Lagois, Phys. Rev. B **23**, 5511 (1981).
[40] J. C. Johnson, H. Yan, R. D. Schaller, P. B. Petersen, P. Yang, and R. J. Saykally, Nano Lett. **2**, 279 (2002).
[41] R. W. Boyd, *Nonlinear Optics* (Academic, New York, 2003).
[42] R. Prasanth, L. K. van Vugt, D. A. M. Vanmaekelbergh, and H. C. Gerritsen, Appl. Phys. Lett. **88**, 181501 (2006).